View metadata, citation and similar papers at core.ac.uk

brought to you by CORE

provided by K-State Research Exchange

Hindawi Publishing Corporation
International Journal of Photoenergy
Volume 2013, Article ID 685614, 10 pages
http://dx.doi.org/10.1155/2013/685614

Research Article

Au-TiO_2 Nanocomposites and Efficient Photocatalytic Hydrogen Production under UV-Visible and Visible Light Illuminations: A Comparison of Different Crystalline Forms of TiO_2

Deepa Jose,[1] Christopher M. Sorensen,[2] Sadhana S. Rayalu,[1,3] Khadga M. Shrestha,[1] and Kenneth J. Klabunde[1]

[1] *Department of Chemistry, Kansas State University, Manhattan, KS 66506, USA*
[2] *Department of Physics, Kansas State University, Manhattan, KS 66506, USA*
[3] *Environmental Materials Division, National Environmental Engineering Research Institute (CSIR-NEERI), Nehru Marg, Nagpur, Maharashtra 440020, India*

Correspondence should be addressed to Kenneth J. Klabunde; kenjk@ksu.edu

Received 14 January 2013; Revised 5 March 2013; Accepted 11 March 2013

Academic Editor: Elias Stathatos

Copyright © 2013 Deepa Jose et al. This is an open access article distributed under the Creative Commons Attribution License, which permits unrestricted use, distribution, and reproduction in any medium, provided the original work is properly cited.

$Au_{(\sim 1\,wt\%)}/TiO_{2(anatase\ or\ rutile\ or\ P25)}$ nanocomposites were prepared by the solvated metal atom dispersion (SMAD) method, and the as-prepared samples were characterized by diffuse reflectance UV-visible spectroscopy, powder XRD, BET surface analysis measurements, and transmission electron microscopy bright field imaging. The particle size of the embedded Au nanoparticles ranged from 1 to 10 nm. These Au/TiO_2 nanocomposites were used for photocatalytic hydrogen production in the presence of a sacrificial electron donor like ethanol or methanol under UV-visible and visible light illumination. These nanocomposites showed very good photocatalytic activity toward hydrogen production under UV-visible conditions, whereas under visible light illumination, there was considerably less hydrogen produced. Au/P25 gave a hydrogen evolution rate of 1600 μmol/h in the presence of ethanol (5 volume %) under UV-visible illumination. In the case of Au/TiO_2 prepared by the SMAD method, the presence of Au nanoparticles serves two purposes: as an electron sink gathering electrons from the conduction band (CB) of TiO_2 and as a reactive site for water/ethanol reduction to generate hydrogen gas. We also observed hydrogen production by water splitting in the absence of a sacrificial electron donor using Au/TiO_2 nanocomposites under UV-visible illumination.

1. Introduction

Ever since the first report of water splitting using a TiO_2 photoanode by Fujishima and Honda, researchers all over the world have been trying to develop efficient solar energy harvesting semiconductor materials for water splitting and thereby producing clean hydrogen energy [1]. Several strategies like band gap engineering of semiconductor materials, cocatalyst loading, two-step photoexcitation (Z scheme), and so forth have been developed to achieve efficient overall water splitting to produce hydrogen and oxygen [2–5]. Recently, people have been trying to exploit the UV and visible absorption of metal nanoparticles like Au, Ag, and Cu by embedding them on a semiconductor material [6, 7]. Among the various semiconductor catalysts, TiO_2 is one of the most promising due to its high chemical stability, nontoxicity, and low cost [8]. The only limitation of TiO_2 as a photocatalyst is its poor efficiency in the visible region of the solar spectrum due to its wide band gap (3.2 eV for anatase). However, TiO_2 can show some visible photocatalytic activity due to the presence of some rutile form of TiO_2 and/or by doping it with metal or nonmetallic elements [9–11] or by deposition of noble metal nanoparticles on TiO_2 [12–15]. Metal nanoparticle loaded TiO_2 showed enhanced photocatalytic activity under UV or visible light illumination. The improved UV activity of these photocatalysts is attributed to the better charge separation by electron transfer from the conduction band (CB) of TiO_2 to Au nanoparticles [16–18], whereas the observed visible activity is explained as photoexcitation of Au nanoparticles (due to surface plasmon resonance effect) and charge separation

by the transfer of photoexcited electrons from Au to the CB of TiO_2 [16, 19–25]. There are some other reports explaining the enhanced visible activity of Au/TiO_2 due to local electric field enhancement near the TiO_2 surface by the Au surface plasmon resonance [26–29].

There are several methods reported in the literature for the synthesis of TiO_2 supported gold nanoparticles such as adsorption of preformed Au colloids [30], photodeposition [31, 32], deposition precipitation [33], impregnation [33], and chemical reduction [34]. We used a different approach for the synthesis of these Au loaded TiO_2 nanocomposites: the solvated metal atom dispersion (SMAD) method. The SMAD technique has been used extensively in our laboratories for the gram scale synthesis of nanoparticles of metals like Au, Ag, Cu, metal chalcogenides, [35–38]. The advantages of this method over other routes reported in the literature are that no byproducts are formed, reproducibility and scalability. We used different types of TiO_2: anatase (UV active), rutile (visible active), and P25 (a mixture of 75% anatase and 25% rutile) for Au loading. These Au (~1 wt%) loaded TiO_2 nanocomposites, prepared by the SMAD method were used as photocatalysts toward photocatalytic hydrogen production, in the presence or absence of a sacrificial electron donor ethanol (5 volume%) under UV-visible and visible conditions. This paper will discuss our findings regarding the role of Au nanoparticles and the role of different crystalline forms of TiO_2.

2. Materials and Methods

2.1. Materials. The different phases of TiO_2 used were anatase (Alfa Aesar, 99.9% and anatase prepared by aerogel method in our laboratories), rutile (Sigma Aldrich, 99.99%), and P25 (Degussa). Sodium sulfite (98.3%) was purchased from Fischer Scientific. Butanone (Sigma Aldrich, 99.7%) was distilled and freeze pump thaw processed for five cycles prior to use in SMAD experiments. Ethanol (200 Proof) from Decon Labs was used for photochemical reactions.

2.2. Instrumentation. Diffuse reflectance UV-visible spectra (DRS UV) were recorded using a Cary 500 scan UV-Vis-NIR spectrophotometer operating in air at room temperature over the range from 200 to 800 nm. Brunauer-Emmet-Teller (BET) measurements of surface area and pore size distribution of TiO_2 and Au/TiO_2 nanocomposites were determined using a Quantachrome NOVA 1200 N_2 gas adsorption/desorption analyzer at liquid nitrogen temperature. Powder XRD analysis of these samples was carried out using a Scintag-XDS-2000 spectrometer with Cu Kα radiation with applied voltage of 40 kV and current of 40 mA. TEM bright filed images were taken using a Phillips CM100 electron microscope operating at 100 kV. Bulk elemental analysis was carried out using Perkin Elmer Optima 4300DV spectrometer (ICP-OES) at Galbraith laboratories Inc.

2.3. Preparation of Au/TiO_2 Nanocomposites. Au loaded TiO_2 nanocomposites were prepared by the SMAD method. The details of the SMAD technique are given elsewhere [39]. In a typical experiment, the crucible was loaded with Au shot (~60 mg) and TiO_2 (P25, anatase commercial, anatase aerogel, or rutile) (~2960 mg) was placed in the bottom of the reactor. Liquid nitrogen cooling and vacuum were applied to the reactor and the crucible was heated resistively under vacuum in such a manner that there was cocondensation of Au atoms with solvent molecules (butanone) on the walls of the reactor. The reactor was brought up to room temperature under Ar atmosphere once the metal evaporation was complete. Upon matrix (Au-butanone) melt down, the Au-butanone colloid comes into contact with TiO_2 at the bottom of the reactor. The Au-butanone/TiO_2 mixture was stirred vigorously under Ar atmosphere for 2 h. The color of the slurry changed from dark blue to purple during the stirring process. Butanone was removed from the mixture by applying vacuum, and the dried powder was used for further studies. In addition to the vacuum drying, Au/TiO_2 samples for control experiments were calcined in air at 200°C for 2 h (heating rate, 5°C/min) to make sure that there was no butanone remaining. The catalysts prepared by the SMAD method are shown in Figure S1 (see Supplementary Material available online at doi: http://dx.doi.org/ 10.1155/2013/685614), and their color varied from lavender to purple.

2.4. Photocatalytic Water Splitting Experiments Using a 450 W Mercury Lamp. The photocatalytic water splitting experiments were carried out in a glass enclosed reaction chamber with a quartz inner radiation reaction vessel. The glass chamber was connected to a gas circulation evacuation and water cooling system. In a typical experiment, 255 mg catalyst (as prepared Au/TiO_2 or Au/TiO_2 calcined at 200°C for 2 h), 322 mL distilled water, and 18 mL ethanol (or 18 mL methanol or 20 mM sodium sulfite) as sacrificial electron donor was taken in the glass reactor with a magnetic stir bar. The reaction mixture was evacuated and filled with Ar five times to remove all the dissolved gases. This was followed by irradiation using a 450 W high pressure Hg lamp via a quartz tube. Water at 20°C was circulated continuously through the outer walls of the reactor and the quartz vessel to make sure that the temperature of the reaction mixture did not exceed 35°C [40]. The activity of these catalysts for hydrogen production was investigated during the first 5 h irradiation period, using a fresh catalyst each time. 2 M $NaNO_2$ solution was used as a filter to cut off UV radiation in our visible studies (UV-visible absorption spectrum of 2 M $NaNO_2$ is given in the supporting information). H_2 production was monitored using an online GC system (GOW-MAC 580 model) employing an All Tech molecular 80/100 sieve 5 A column with Ar as the carrier gas and a thermal conductivity detector.

3. Results and Discussions

3.1. Au/TiO_2 Nanocomposites Characterization. Au nanoparticles (~1 wt%) loaded on to a variety of anatase, rutile, and a mixture of anatase and rutile (P25) TiO_2 were prepared by the SMAD method. The as-prepared samples were characterized by diffuse reflectance UV-visible spectroscopy, BET surface area analysis, transmission electron microscopy, and

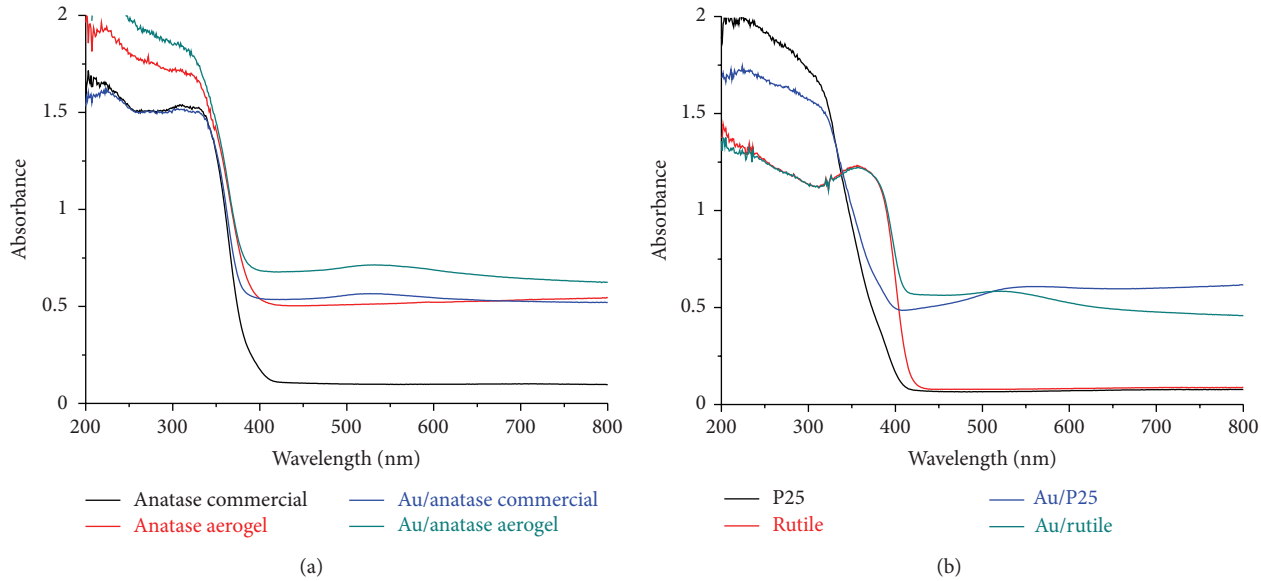

FIGURE 1: Diffuse reflectance UV-visible spectra of Au/TiO_2 photocatalysts prepared by the SMAD method.

powder XRD. The diffuse reflectance spectra of Au/TiO_2 nanocomposites showed 2 sets of peaks (Figure 1): band gap transition band of TiO_2 with a maximum in the UV region and surface plasmon resonance band in the visible region (Au/anatase commercial with a maxima at 526 nm, Au/anatase aerogel with a maxima at 535 nm, Au/rutile with a maxima at 525 nm, and Au/P25 with a maxima at 560 nm). The position and shape of the surface plasmon resonance band depends on particle size, shape, and dielectric constant of the medium [41]. The red shift of the surface plasmon band maxima in these nanocomposites can be attributed to the refractive index of the TiO_2 matrix. The band gap values of the respective phases of TiO_2 remained unchanged even after Au loading as per the DRS UV data (anatase = 3.2 eV, rutile = 3.0 eV, and P25 = 3.1 eV).

The presence of loaded Au nanoparticles on the TiO_2 matrix was confirmed by TEM bright field imaging. The TEM bright field images of different phases of TiO_2 before and after Au loading are given in Figures 2 and 3. Commercial anatase has micron sized particles (0.1-0.2 μm, Figure 2(a)) with a surface area 13 m^2/g, whereas anatase prepared by the aerogel method consists of small nanometer sized particles (10–15 nm, Figure 2(b)) with a high surface area of 102 m^2/g (Figure S1 and Table S1). TEM bright field images of these anatase particles showed embedded Au nanoparticles of size ranging from 1 to 9 nm (Figures 2(c) and 2(d)) with an average particle diameter of 2.4 nm and 4.3 nm (Figure 4) for aerogel and commercial anatase, respectively. The surface areas of these Au/anatase nanocomposites were less than the respective TiO_2 matrix used (Table S1). The rutile phase of TiO_2 used in our studies showed micron sized particles (0.2–0.6 μm, Figure 3(c)). The surface area of rutile was found to be very low (Table S1). The TEM bright field image (Figure 3(d)) showed embedded Au nanoparticles on the semiconductor with a size ranging from 3 to 8 nm with an average particle diameter of 4.7 nm (Figure 4). In the case of P25, the particles size ranged from 15 to 20 nm (Figure 3(a)) with a surface area of about 48 m^2/g (Table S1). TEM bright field images exhibited Au nanoparticles of size ranging from 3 to 10 nm (Figure 3(b)) with an average particle diameter of 6.7 nm (Figure 4). The powder XRD pattern (Figure S3) of these Au/TiO_2 nanocomposites did not show any Au reflections due to the low concentration (Table S2) of Au in these samples.

A conclusion from these characterization studies is that the final gold particle size depends a great deal on the surface area of the TiO_2 support. Therefore, as the Au-butanone colloid encountered the cold TiO_2, gold nanoparticle growth is limited/controlled by the TiO_2 surface available.

3.2. Photocatalytic Activity of Au/TiO_2 Nanocomposites under UV-Visible Conditions. All Au/TiO_2 photocatalysts prepared by our SMAD method showed UV-visible activity to generate hydrogen in the presence of a sacrificial electron donor, irrespective of the TiO_2 phase present in the system (Table 1). Among the different catalysts used, Au/P25 showed the highest activity with a hydrogen production rate of 1600 μmol/h in the presence of ethanol. In addition to ethanol as a sacrificial agent, we used methanol and sodium sulfite as an electron scavenger in Au/P25 system. The rate of hydrogen evolution was lower compared to ethanol when methanol was used as the sacrificial agent with a photocatalytic hydrogen production of 816 μmol/h. The photocatalytic hydrogen production was very low when 20 mM sodium sulfite solution was used as a sacrificial agent (20 μmol/h). These results clearly indicate that during sacrificial electron donor mediated hydrogen production, there is a considerable contribution toward hydrogen generation from the sacrificial agent in addition to the hydrogen generation.

Au/TiO_2 photocatalysts were found to be much more active compared to their samples without gold. The higher activity could be attributed to the better charge separation

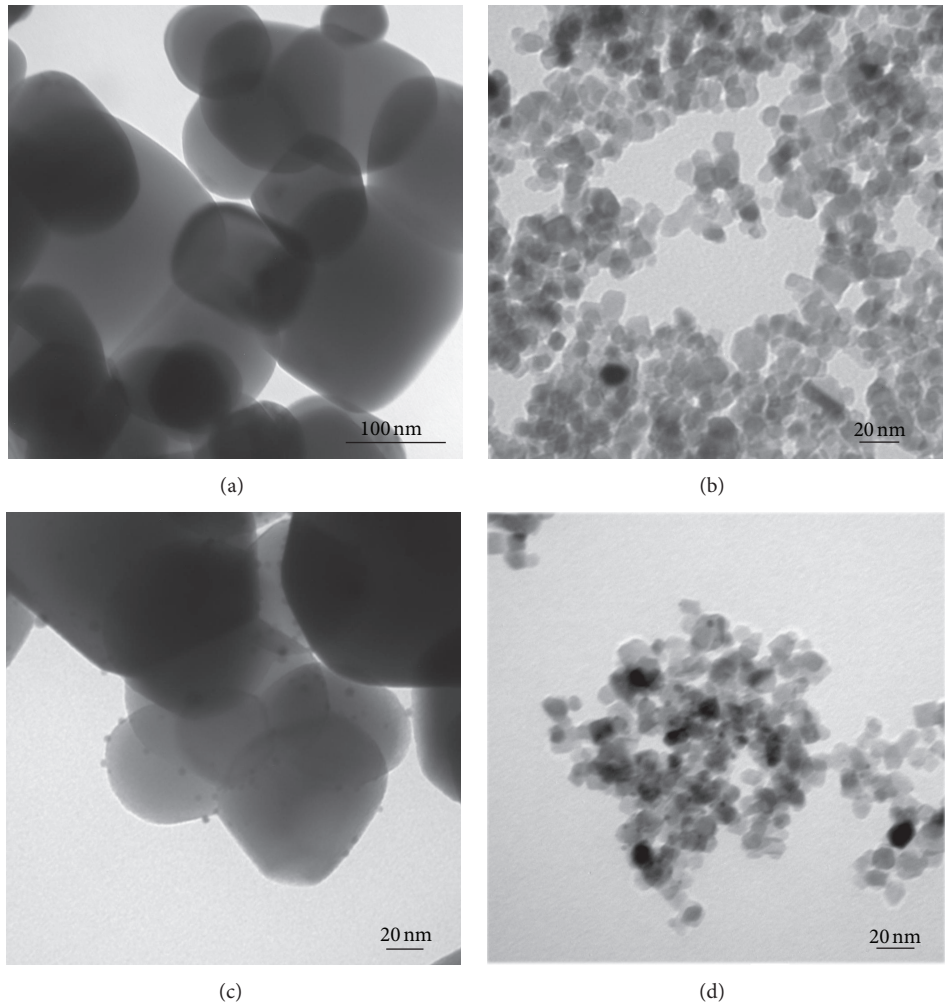

Figure 2: TEM bright field images of anatase phase of TiO_2 before and after Au loading (a) anatase commercial, (b) anatase aerogel, Au/TiO_2 (c) Au/anatase commercial, and (d) Au/anatase aerogel.

Table 1: Amount of hydrogen evolved using Au/TiO_2 nanocomposites under dark, visible, and UV-visible photocatalytic runs for 5 h in the presence of ethanol (5 volume%) using a 450 W Mercury lamp.

Catalyst	Rate (μmol/h)		
	Dark	Visible	UV-visible
No catalyst	0.0	0.0	2.2
P25	0.0	1.9	90
Au/P25	0.0	6.9	1600
Anatase commercial	0.0	0.0	1.7
Au/anatase commercial	0.0	0.0	300
Anatase aerogel	0.0	0.0	18
Au/anatase aerogel	0.0	0.0	1200
Rutile	0.0	3.3	6.3
Au/rutile	0.0	5.6	530

achieved in these catalysts where Au particles are good electron scavengers as well as catalyst surfaces for hydrogen formation. The subsequent holes in photoexcited TiO_2 are quenched by the sacrificial electron donor ethanol. The Fermi level of Au nanoparticles (E_F = +0.45 V versus NHE at pH 7 for bulk Au) is more positive than the bottom of the conduction band of TiO_2 (E_{CB} = −0.5 V versus NHE at pH 7) which favors the electron transfer from photoexcited TiO_2 to Au. However, the reduction potential of water is −0.41 V (NHE at pH 7), and the transferred electrons cannot reduce water until the Fermi level of Au is raised to negative potentials. There are several reports in the literature regarding metal nanoparticle storing electrons in its Fermi level and shifting the Fermi level to more negative potentials when they come into contact with a photoexcited semiconductor nanoparticle like TiO_2 [17, 18, 42–46]. This kind of electron transfer from semiconductor to metal continues until Fermi level equilibration takes place. Choi et al. showed that under UV irradiation, Au@TiO_2 core-shell nanoparticles exhibit a blue shift in the surface plasmon resonance band maxima due to the transfer of electrons from TiO_2 to Au core and the Fermi level shift to negative potentials [47]. Au cannot undergo this kind of the Fermi level shift without taking electrons from a semiconductor [47].

3.3. Photocatalytic Activity of TiO_2 and Au/TiO_2 Nanocomposites under Visible Conditions. We used 2 M $NaNO_2$ solution as a filter to cut off the UV radiations under our

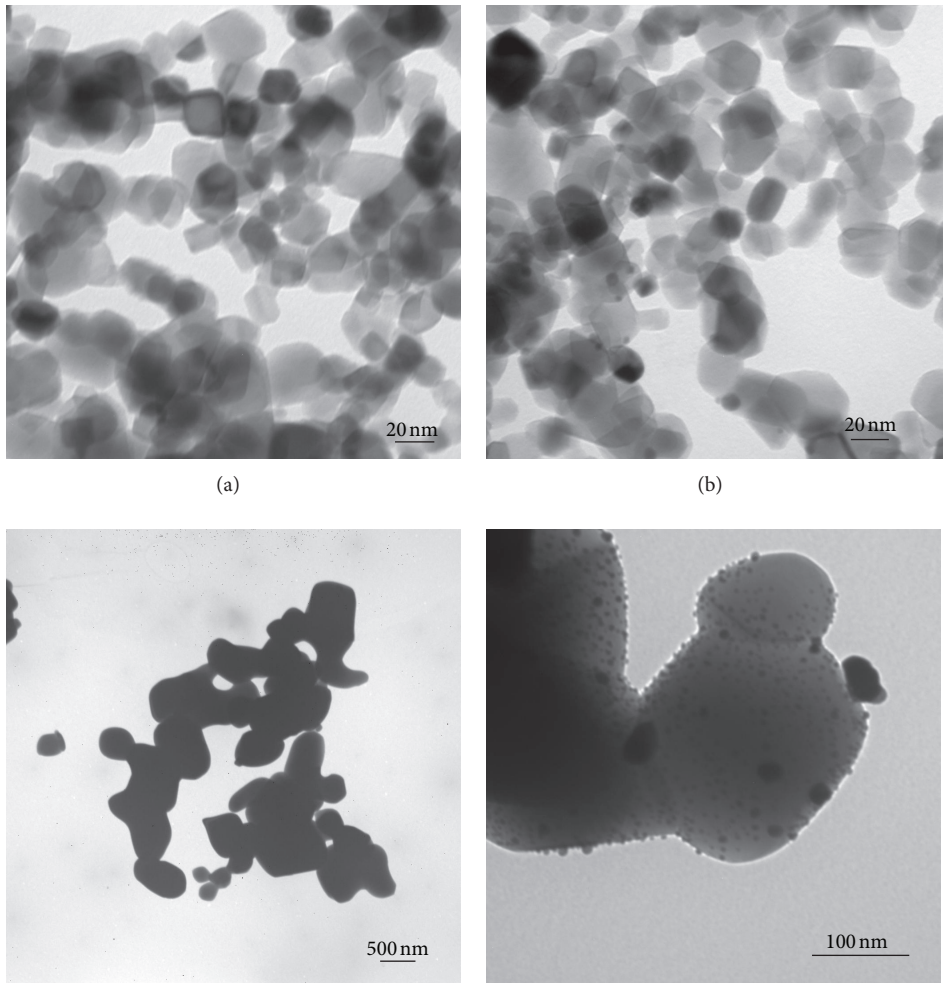

(a) (b)

(c) (d)

Figure 3: TEM bright field images of (a) P25, (b) Au/P25, (c) rutile, and (d) Au/rutile.

visible light illumination photocatalytic experiments. From the UV-visible spectrum of $NaNO_2$ (Figure S4) it is clear that this chemical filter cuts off radiation only up to 400 nm. Since rutile does absorb in the 400–410 nm range, some charge transfer from TiO_2 to Au could take place. As expected, the rutile phase of TiO_2 is visible light active, whereas the anatase phase is visible light inactive due to its slightly large band gap. Au loading improved the visible light activity of TiO_2 nanoparticles containing the rutile phase. Thus, the enhanced visible activity of these rutile-containing photocatalysts could be due to better charge separation in the presence of Au nanoparticles by transferring electrons from the CB of TiO_2 to the Au Fermi level [16–18].

In addition to the charge transfer from TiO_2 to Au, there are several reports where Au imparts visible activity to wide band gap visible light inactive semiconductor nanoparticles like TiO_2, $SrTiO_3$, and CeO_2 [19–25, 48–51]. García and coworkers prepared visible active Au loaded P25 or CeO_2 nanocomposites for hydrogen or oxygen production by water splitting in the presence of a sacrificial electron donor (methanol or EDTA) or acceptor [16, 48]. According to these reports, Au nanoparticles absorb visible light by the surface plasmon resonance effect; charge separation at the Au nanoparticle takes place by the transfer of excited electrons from Au to the CB of TiO_2; subsequent holes are quenched by the sacrificial electron donor. Kimura et al. showed that the rutile form of TiO_2 more favors this kind of interfacial electron transfer from Au to TiO_2 [19]. Essentially, in these reported systems, Au nanoparticle acts as a sensitizer as in the case of dye-sensitized solar cells [49].

However, this kind of electron transfer from Au to the CB of TiO_2 is not energetically favored [26]. On the other hand, Tian and Tatsuma showed that this kind of electron transfer is possible due to the formation of a Schottky barrier at Au/TiO_2 junctions [20, 50]. In the case of $Pt_{(05\,wt\%)}/SrTiO_3$, the Pt metal decreases the band gap energy of $SrTiO_3$ by the formation of a Schottky barrier at the $Pt/SrTiO_3$ interface [51]. Thus, there is still controversy regarding electron flow to or from metal particles with TiO_2.

To get a better overall understanding about how Au nanoparticles impart visible activity to TiO_2 semiconductor, we examined the visible activity of Au/anatase nanocomposites. Two different types of anatase were used: a commercial one with micron sized particles and anatase prepared by an

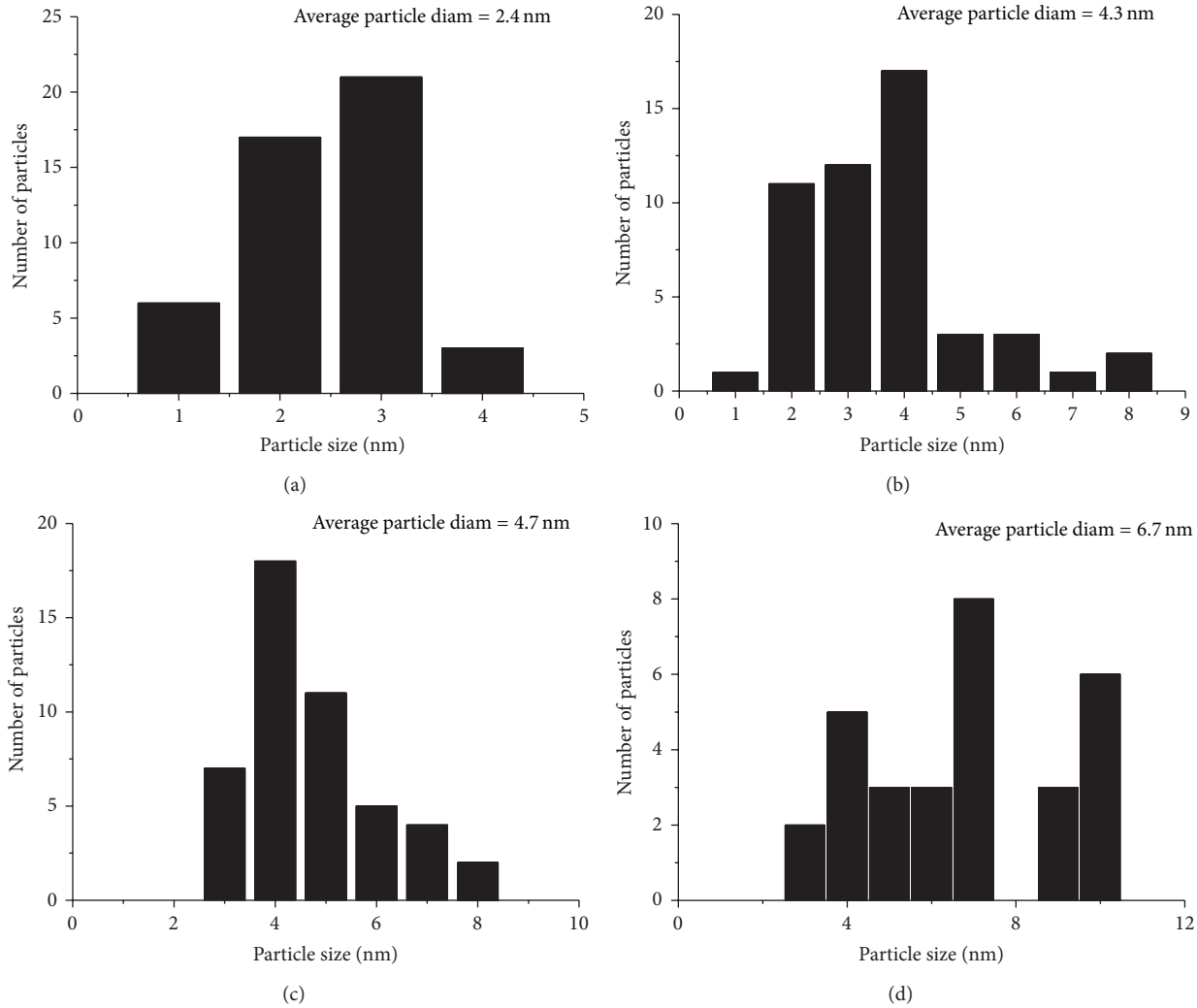

Figure 4: Histogram showing particle size distribution of Au nanoparticles loaded onto different phases of TiO_2 nanoparticles (a) Au/Anatase aerogel, (b) Au/anatase commercial, (c) Au/rutile, and (d) Au/P25.

aerogel method with nanometer sized particles. Regardless of the anatase used for Au loading, we did not see any visible light activity for the first five hours in the presence of water ethanol mixture. However, there was a very small amount of hydrogen evolution sixth-hour onwards. The mechanism of formation of small amount of hydrogen after five hours of visible light illumination is not clear to us, which could be either due to the reduction of water or due to the thermal decomposition of ethanol, aided by small nanoparticles undergoing nonradiative decay forming localized hot spots [52, 53].

It has also been reported that Au nanoparticles can also impart visible activity to a plasmonic-metal/semiconductor nanocomposite by surface plasmon mediated local electric field enhancement [26–29]. Interaction of a semiconductor nanoparticle with this kind of localized electric field could allow the formation of electron/hole pairs in the near surface region which can migrate to the surface without undergoing electron/hole pair recombination. For example, electromagnetic simulations showed that the increased photocatalytic water splitting under visible illumination of anodic TiO_2 with Au nanoparticles is due to the local electric field enhancement near the TiO_2 surface instead of electron transfer from Au to the CB of TiO_2 [26]. Awazu et al. called this kind of surface plasmon-induced localized electric field enhancement and improved photocatalytic activity as "plasmonic photocatalysis" [54]. Christopher et al. explained the enhanced visible activity of Ag/TiO_2 as due to the higher concentration of charge carriers in the semiconductor by plasmon mediated radiative transfer of energy from Ag nanoparticles to TiO_2, no electron flow from Ag to TiO_2 was observed [55]. Recently, Seh et al. showed enhanced visible light activity for the Janus shaped anatase $Au\text{-}TiO_2$ nanocomposites as due to the strong localization of plasmonic near fields close to the $Au\text{-}TiO_2$ interface and the coupling of plasmonic near fields to optical transitions involving localized electronic states in amorphous TiO_2 [29]. In our case, this kind of localized electric field created by Au nanoparticles could not generate electron/hole pairs in the near surface region of the semiconductor as the surface plasmon absorbance of Au

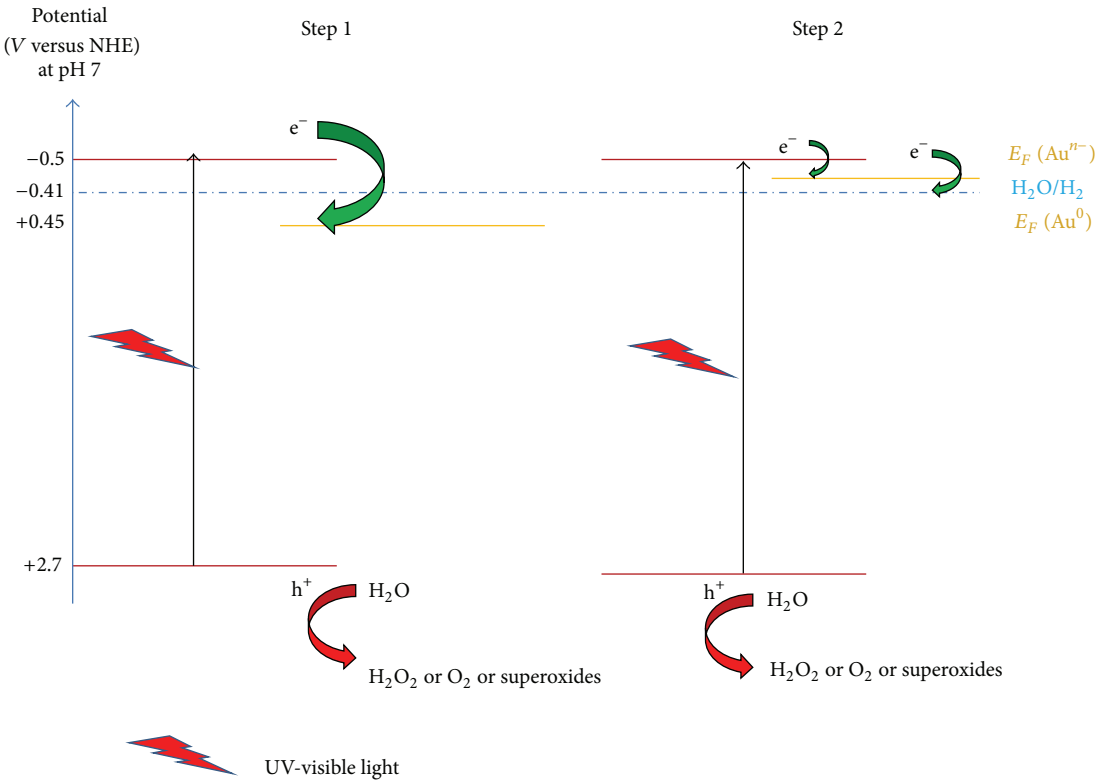

Scheme 1: Elementary steps showing photocatalytic water splitting under UV-visible illumination using Au/TiO_2 nanocomposites: step 1 is electron transfer from the CB of photoexcited TiO_2 to the Au Fermi level, and step 2 is the Au Fermi level shift to negative potential by gathering photoexcited electrons from TiO_2 and water reduction.

nanoparticle does not overlap with the TiO_2 absorption spectrum. Linic and Ingram observed enhanced visible activity with Ag loaded N-TiO_2, whereas Au loaded N-TiO_2 did not show any significant enhancement in the photocurrent due to the red shift in the position of surface plasmon absorption band of Au nanoparticles compared to that of Ag [56].

3.4. Au Nanoparticles in Au/TiO_2 Nanocomposites Act as an Electron Sink for Better Charge Separation and Total Water Splitting. Our results indicate that there is a transfer of electrons from TiO_2 to Au and Au nanoparticle acts as a sink for photogenerated electrons. If this is true, Au nanoparticles could aid charge separation without using a sacrificial electron donor. We strengthened this hypothesis by doing photocatalytic water splitting under UV-visible conditions using Au/P25 nanocomposites in the absence of a sacrificial electron donor. There was an evolution of hydrogen (Figure 5) which again supports the proposed mechanism of charge separation achieved by Au nanoparticles (acts as a sink for photogenerated electrons and the Fermi level equilibration) and water molecules (quench the holes in the valence band of TiO_2). In order to prove that the hydrogen evolution is not caused by some organic impurities like butanone incorporated into the Au/P25 photocatalyst during sample preparation, we used calcined Au/P25 (at 200°C for 2 h). This sample showed photocatalytic activity for several cycles (Figure 5). We also did control experiments, wherein we used Degussa P25 and tried photocatalytic water splitting

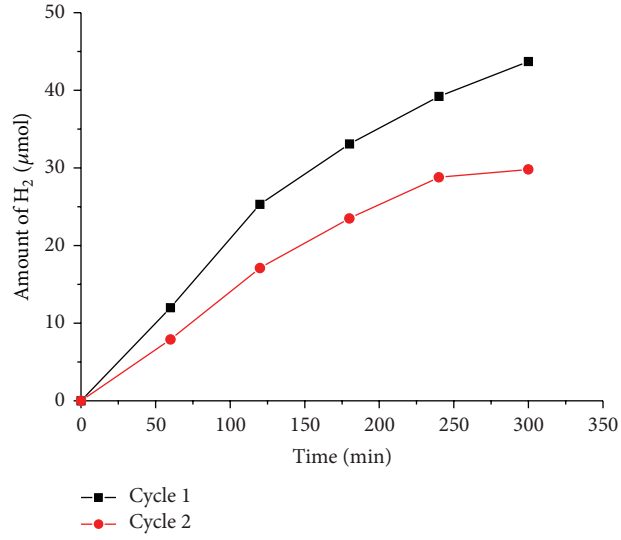

Figure 5: Hydrogen evolution by photocatalytic water splitting in the absence of sacrificial electron donor using Au/P25 (calcined sample) under UV-visible conditions.

in the absence of ethanol; there was no hydrogen evolution. These results imply a mechanism shown in Scheme 1.

The rate of hydrogen evolution was low for Au/P25 in the absence of ethanol. P25 produced no hydrogen in the absence of ethanol; however, in the presence of ethanol, there

was hydrogen evolution. This implies two things: (1) charge separation in pure TiO_2 takes place only in the presence of a sacrificial electron donor; (2) charge separation takes place in TiO_2 nanoparticles which are in good interfacial contact with Au nanoparticles even in the absence of a sacrificial electron donor. In the absence of ethanol, initially, charge separation takes place only on those TiO_2 particles which are in good interfacial contact with Au nanoparticles by transferring photoelectrons from the CB of TiO_2 to the Au Fermi level; holes are being quenched by water molecules to produce H_2O_2 or O_2. Thus, charge separation takes place in the case of photoexcited TiO_2 nanoparticles which are in good interfacial contact with TiO_2, and the Au/TiO_2 Fermi level equilibration takes place. Subsequent water reduction and hydrogen evolution are observed. The amount of hydrogen evolved in the absence of ethanol is low compared to the hydrogen evolved in the presence of ethanol. This could be due to the low concentration (1 wt%) of Au (which causes the charge separation) in these catalysts. We could not see any oxygen evolution during these experiments. This could be due to several reasons: (1) the reaction mixture was deaerated before photoillumination, and evolved small amount of oxygen could dissolve in water due to the high solubility of oxygen in water compared to hydrogen [57], (2) evolved oxygen can accept photoexcited electron from TiO_2 to form $O_2^{-\bullet}$ [58, 59]. The rate of the hydrogen evolution decreases with time as the evolved oxygen acts as a better electron acceptor to form superoxide.

4. Conclusions

These Au/TiO_2 photocatalysts were found to be resilent photocatalysts for the generation of hydrogen under UV-visible conditions. The photocatalytic hydrogen evolution rate was found to be 1600 μmol/h which is higher than Au/TiO_2 nanocomposites prepared by the photodeposition method (in our hands). Comparisons of different TiO_2 crystalline forms with different surface areas suggest that, in our case, the best explanation of any visible light activity is that the rutile form can absorb some energetic visible light, and then electrons are scavenged by the Au nanoparticles. This is the same mechanism as with more energetic UV light, where the process is much more efficient.

When ethanol scavenger is present, these photocatalysts are long lived. In the absence of ethanol, catalyst degradation takes place slowly (over days); this process of degradation is not understood, and hydrogen generation is much slower.

Further work comparing different metal nanoparticles is underway.

Conflict of Interests

The authors declare no financial conflict of interests.

Acknowledgments

The authors are grateful to the Department of Energy (Basic Energy Sciences, DE-SC 0005159) for funding. They thank Dr. Dan Boyle for assistance with TEM measurements.

References

[1] A. Fujishima and K. Honda, "Electrochemical photolysis of water at a semiconductor electrode," *Nature*, vol. 238, no. 5358, pp. 37–38, 1972.

[2] K. Maeda, "Photocatalytic water splitting using semiconductor particles: history and recent developments," *Journal of Photochemistry and Photobiology C*, vol. 12, no. 4, pp. 237–268, 2011.

[3] K. Maeda and K. Domen, "Photocatalytic water splitting: recent progress and future challenges," *Journal of Physical Chemistry Letters*, vol. 1, no. 18, pp. 2655–2661, 2010.

[4] R. Abe, "Recent progress on photocatalytic and photoelectrochemical water splitting under visible light irradiation," *Journal of Photochemistry and Photobiology C*, vol. 11, no. 4, pp. 179–209, 2010.

[5] A. Kubacka, M. Fernández-García, and G. Colón, "Advanced nanoarchitectures for solar photocatalytic applications," *Chemical Society Reviews*, vol. 112, no. 3, pp. 1555–1614, 2012.

[6] S. Linic, P. Christopher, and D. B. Ingram, "Plasmonic-metal nanostructures for efficient conversion of solar to chemical energy," *Nature Materials*, vol. 10, pp. 911–921, 2011.

[7] S. C. Warren and E. Thimsen, "Plasmonic solar water splitting," *Energy Environmental Science*, vol. 5, pp. 5133–5146, 2012.

[8] O. Carp, C. L. Huisman, and A. Reller, "Photoinduced reactivity of titanium dioxide," *Progress in Solid State Chemistry*, vol. 32, no. 1-2, pp. 33–177, 2004.

[9] V. Brezová, A. Blažková, L. Karpinský et al., "Phenol decomposition using M^{n+}/TiO_2 photocatalysts supported by the sol-gel technique on glass fibres," *Journal of Photochemistry and Photobiology A*, vol. 109, no. 2, pp. 177–183, 1997.

[10] X. Wang, M. Blackford, K. Prince, and R. A. Caruso, "Preparation of boron-doped porous titania networks containing gold nanoparticles with enhanced visible-light photocatalytic activity," *ACS Applied Materials and Interfaces*, vol. 4, no. 1, pp. 476–482, 2012.

[11] D. B. Hamal and K. J. Klabunde, "Synthesis, characterization, and visible light activity of new nanoparticle photocatalysts based on silver, carbon, and sulfur-doped TiO_2 ," *Journal of Colloid and Interface Science*, vol. 311, no. 2, pp. 514–522, 2007.

[12] A. Primo, A. Corma, and H. García, "Titania supported gold nanoparticles as photocatalyst," *Physical Chemistry Chemical Physics*, vol. 13, no. 3, pp. 886–910, 2011.

[13] X. Wang and R. A. Caruso, "Enhancing photocatalytic activity of titania materials by using porous structures and the addition of gold nanoparticles," *Journal of Materials Chemistry*, vol. 21, no. 1, pp. 20–28, 2011.

[14] H. Tada, T. Kiyonaga, and S. I. Naya, "Rational design and applications of highly efficient reaction systems photocatalyzed by noble metal nanoparticle-loaded titanium(iv) dioxide," *Chemical Society Reviews*, vol. 38, no. 7, pp. 1849–1858, 2009.

[15] V. Subramanian, E. Wolf, and P. V. Kamat, "Semiconductor-metal composite nanostructures. To what extent do metal nanoparticles improve the photocatalytic activity of TiO_2 films?" *Journal of Physical Chemistry B*, vol. 105, no. 46, pp. 11439–11446, 2001.

[16] C. G. Silva, R. Juá rez, T. Marino, R. Molinari, and H. García, "Influence of excitation wavelength (UV or visible light) on the photocatalytic activity of titania containing gold nanoparticles for the generation of hydrogen or oxygen from water," *Journal of the American Chemical Society*, vol. 133, no. 3, pp. 595–602, 2011.

[17] V. Subramanian, E. E. Wolf, and P. V. Kamat, "Catalysis with TiO_2/Gold nanocomposites. Effect of metal particle size on the fermi level equilibration," *Journal of the American Chemical Society*, vol. 126, no. 15, pp. 4943–4950, 2004.

[18] M. Jakob, H. Levanon, and P. V. Kamat, "Charge distribution between UV-irradiated TiO_2 and gold nanoparticles: determination of shift in the Fermi level," *Nano Letters*, vol. 3, no. 3, pp. 353–358, 2003.

[19] K. Kimura, S. I. Naya, Y. Jin-nouchi, and H. Tada, "TiO_2 crystal form-dependence of the Au/TiO_2 plasmon photocatalyst's activity," *Journal of Physical Chemistry C*, vol. 116, no. 12, pp. 7111–7117, 2012.

[20] Y. Tian and T. Tatsuma, "Mechanisms and applications of plasmon-induced charge separation at TiO_2 films loaded with gold nanoparticles," *Journal of the American Chemical Society*, vol. 127, no. 20, pp. 7632–7637, 2005.

[21] D. Tsukamoto, Y. Shiraishi, Y. Sugano, S. Ichikawa, S. Tanaka, and T. Hirai, "Gold nanoparticles located at the interface of anatase/rutile TiO_2 particles as active plasmonic photocatalysts for aerobic oxidation," *Journal of American Chemical Society*, vol. 134, no. 14, pp. 6309–6315, 2012.

[22] A. Furube, L. Du, K. Hara, R. Katoh, and M. Tachiya, "Ultrafast plasmon-induced electron transfer from gold nanodots into TiO_2 nanoparticles," *Journal of the American Chemical Society*, vol. 129, no. 48, pp. 14852–14853, 2007.

[23] Y. Nishijima, K. Ueno, Y. Kotake, K. Murakoshi, H. Inoue, and H. Misawa, "Near-infrared plasmon-assisted water oxidation," *Journal of Physical Chemistry Letters*, vol. 3, no. 10, pp. 1248–1252, 2012.

[24] Y. Nishijima, K. Ueno, Y. Yokota, K. Murakoshi, and H. Misawa, "Plasmon-assisted photocurrent generation from visible to near-infrared wavelength using a Au-nanorods/TiO_2 electrode," *Journal of Physical Chemistry Letters*, vol. 1, no. 13, pp. 2031–2036, 2010.

[25] E. Kowalska, O. O. P. Mahaney, R. Abe, and B. Ohtani, "Visible-light-induced photocatalysis through surface plasmon excitation of gold on titania surfaces," *Physical Chemistry Chemical Physics*, vol. 12, no. 10, pp. 2344–2355, 2010.

[26] Z. Liu, W. Hou, P. Pavaskar, M. Aykol, and S. B. Cronin, "Plasmon resonant enhancement of photocatalytic water splitting under visible illumination," *Nano Letters*, vol. 11, pp. 1111–1116, 2011.

[27] H. Wang, T. You, W. Shi, J. Li, and L. Guo, "Au/TiO_2/Au as a plasmonic coupling photocatalyst," *Journal of Physical Chemistry C*, vol. 116, no. 10, pp. 6490–6494, 2012.

[28] Y. Lu, H. Yu, S. Chen, X. Quan, and H. Zhao, "Integrating plasmonic nanoparticles with TiO_2 photonic crystal for enhancement of visible-light-driven photocatalysis," *Energy Environmental Science*, vol. 46, pp. 1724–1730, 2012.

[29] Z. W. Seh, S. Liu, M. Low et al., "Janus Au-TiO_2 photocatalysts with strong localization of plasmonic near-fields for efficient visible-light hydrogen generation," *Advanced Materials*, vol. 24, no. 17, pp. 2310–2314, 2012.

[30] J. Li and H. C. Zeng, "Preparation of monodisperse Au/TiO_2 nanocatalysts via self-assembly," *Chemistry of Materials*, vol. 18, no. 18, pp. 4270–4277, 2006.

[31] T. Soejima, H. Tada, T. Kawahara, and S. Ito, "Formation of au nanoclusters on TiO_2 surfaces by a two-step method consisting of Au(III)-complex chemisorption and its photoreduction," *Langmuir*, vol. 18, no. 11, pp. 4191–4194, 2002.

[32] C. Yogi, K. Kojima, T. Takai, and N. Wada, "Photocatalytic degradation of methylene blue by Au-deposited TiO 2 film under UV irradiation," *Journal of Materials Science*, vol. 44, no. 3, pp. 821–827, 2009.

[33] W.-C. Li, M. Comotti, and F. Schüth, "Highly reproducible syntheses of active Au/TiO_2 catalysts for CO oxidation by deposition-precipitation or impregnation," *Journal of Catalysis*, vol. 237, no. 1, pp. 190–196, 2006.

[34] M. C. Hidalgo, M. Maicu, J. A. Navío, and G. Colón, "Effect of sulfate pretreatment on gold-modified TiO_2 for photocatalytic applications," *Journal of Physical Chemistry C*, vol. 113, no. 29, pp. 12840–12847, 2009.

[35] S. Stoeva, K. J. Klabunde, C. M. Sorensen, and I. Dragieva, "Gram-scale synthesis of monodisperse gold colloids by the solvated metal atom dispersion method and digestive ripening and their organization into two- and three-dimensional structures," *Journal of the American Chemical Society*, vol. 124, no. 10, pp. 2305–2311, 2002.

[36] A. B. Smetana, K. J. Klabunde, and C. M. Sorensen, "Synthesis of spherical silver nanoparticles by digestive ripening, stabilization with various agents, and their 3-D and 2-D superlattice formation," *Journal of Colloid and Interface Science*, vol. 284, no. 2, pp. 521–526, 2005.

[37] A. A. Ponce and K. J. Klabunde, "Chemical and catalytic activity of copper nanoparticles prepared via metal vapor synthesis," *Journal of Molecular Catalysis A*, vol. 225, no. 1, pp. 1–6, 2005.

[38] S. Cingarapu, Z. Yang, C. M. Sorensen, and K. J. Klabunde, "Synthesis of CdSe quantum dots by evaporation of bulk CdSe using SMAD and digestive ripening processes," *Chemistry of Materials*, vol. 21, no. 7, pp. 1248–1252, 2009.

[39] K. J. Klabunde, P. L. Timms, P. S. Skell, and S. Ittel, "Introduction to metal vapor synthesis," *Inorganic Synthesis*, vol. 19, pp. 59–86, 1979.

[40] Y. Kuo, C. D. Frye, M. Ikenberry, and K. J. Klabunde, "Titanium-indium oxy(nitride) with and without RuO_2 loading as photocatalysts for hydrogen production under visible light from water," *Catalysis Today*, vol. 199, pp. 15–23, 2013.

[41] K. L. Kelly, E. Coronado, L. L. Zhao, and G. C. Schatz, "The optical properties of metal nanoparticles: the influence of size, shape, and dielectric environment," *Journal of Physical Chemistry B*, vol. 107, no. 3, pp. 668–677, 2003.

[42] P. V. Kamat, "Manipulation of charge transfer across semiconductor interface. A criterion that cannot be ignored in photocatalyst design," *Journal of Physical Chemistry Letters*, vol. 3, no. 5, pp. 663–672, 2012.

[43] A. Takai and P. V. Kamat, "Capture, store and discharge. Shuttling photogenerated electrons across TiO_2-silver interface," *ACS Nano*, vol. 5, no. 9, pp. 7369–7376, 2011.

[44] V. Subramanian, E. E. Wolf, and P. V. Kamat, "Green emission to probe photoinduced charging events in ZnO-Au nanoparticles. Charge distribution and Fermi-level equilibration," *Journal of Physical Chemistry B*, vol. 107, no. 30, pp. 7479–7485, 2003.

[45] T. Hirakawa and P. V. Kamat, "Photoinduced electron storage and surface plasmon modulation in Ag TiO 2 clusters," *Langmuir*, vol. 20, no. 14, pp. 5645–5647, 2004.

[46] A. Wood, M. Giersig, and P. Mulvaney, "Fermi level equilibration in quantum dot-metal nanojunctions," *Journal of Physical Chemistry B*, vol. 105, no. 37, pp. 8810–8815, 2001.

[47] H. Choi, W. T. Chen, and P. V. Kamat, "Know thy metal neighbor. Plasmonic versus electron charging effects of gold nanoparticles in dye sensitized solar cells," *ACS Nano*, vol. 6, no. 5, pp. 4418–4427, 2012.

[48] A. Primo, T. Marino, A. Corma, R. Molinari, and H. García, "Efficient visible-light photocatalytic water splitting by minute amounts of gold supported on nanoparticulate CeO_2 obtained by a biopolymer templating method," *Journal of the American Chemical Society*, vol. 133, no. 18, pp. 6930–6933, 2011.

[49] B. O'Regan and M. Grätzel, "A low-cost, high-efficiency solar cell based on dye-sensitized colloidal TiO_2 films," *Nature*, vol. 353, no. 6346, pp. 737–740, 1991.

[50] J. Tang, M. White, G. D. Stucky, and E. W. McFarland, "Electrochemical fabrication of large-area Au/TiO_2 junctions," *Electrochemistry Communications*, vol. 5, no. 6, pp. 497–501, 2003.

[51] T. Puangpetch, T. Sreethawong, S. Yoshikawa, and S. Chavadej, "Hydrogen production from photocatalytic water splitting over mesoporous-assembled SrTiO3 nanocrystal-based photocatalysts," *Journal of Molecular Catalysis A*, vol. 312, no. 1-2, pp. 97–106, 2009.

[52] C.-W. Yen and M. A. El-Sayed, "Plasmonic field effect on the hexacyanoferrate (III)-thiosulfate electron transfer catalytic reaction on gold nanoparticles: electromagnetic or thermal?" *Journal of Physical Chemistry C*, vol. 113, no. 45, pp. 19585–19590, 2009.

[53] J. R. Adleman, D. A. Boyd, D. G. Goodwin, and D. Psaltis, "Heterogenous catalysis mediated by plasmon heating," *Nano Letters*, vol. 9, no. 12, pp. 4417–4423, 2009.

[54] K. Awazu, M. Fujimaki, C. Rockstuhl et al., "A plasmonic photocatalyst consisting of silver nanoparticles embedded in titanium dioxide," *Journal of the American Chemical Society*, vol. 130, no. 5, pp. 1676–1680, 2008.

[55] P. Christopher, D. B. Ingram, and S. Linic, "Enhancing photochemical activity of semiconductor nanoparticles with optically active Ag nanostructures: photochemistry mediated by Ag surface plasmons," *Journal of Physical Chemistry C*, vol. 114, no. 19, pp. 9173–9177, 2010.

[56] D. B. Ingram and S. Linic, "Water splitting on composite plasmonic-metal/semiconductor photoelectrodes: evidence for selective plasmon-induced formation of charge carriers near the semiconductor surface," *Journal of the American Chemical Society*, vol. 133, no. 14, pp. 5202–5205, 2011.

[57] http://www.engineeringtoolbox.com/gases-solubility-water–d_1148.html.

[58] J. Kiwi and M. Grätzel, "Optimization of conditions for photochemical water cleavage. Aqueous Pt/TiO_2 (anatase) dispersions under ultraviolet light," *Journal of Physical Chemistry*, vol. 88, no. 7, pp. 1302–1307, 1984.

[59] M. V. Rao, K. Rajeshwar, V. R. Pal Verneker, and J. DuBow, "Photosynthetic production of H_2 and H_2O_2 on semiconducting oxide grains in aqueous solutions," *Journal of Physical Chemistry*, vol. 84, no. 15, pp. 1987–1991, 1980.